RESEARCH PAPER

Seismic fragility analysis of deteriorated bridge structures employing a UAV inspection-based updated digital twin

Sungsik Yoon[1] · Sangmok Lee[2] · Seungkyung Kye[3] · In-Ho Kim[4] · Hyung-Jo Jung[3] · Billie F. Spencer Jr[5]

Abstract

Aging bridges require regular inspection due to performance deterioration. For this purpose, numerous researchers have considered the use of unmanned aerial vehicle (UAV) systems for structural health monitoring and inspection. However, present UAV-based inspection methods only represent the type and extent of external damage, but does not assess the seismic performance. In this study, a seismic fragility analysis of deteriorated bridges employing a UAV inspection-based updated digital twin is proposed. The proposed method consists of two phases: (1) bridge condition assessment using UAV inspection for updating the digital twin and (2) seismic fragility analysis based on the updated digital twin. To update the digital twin, the bridge damage grade is assigned based on the UAV inspection, and subsequently, the corresponding damage index is calculated. The damage index is utilized as a percentage reduction in the stiffness of finite element (FE) model, based on a previously proposed research. Using the updated digital twin, the seismic fragility analysis is conducted with different earthquake motions and magnitudes. To demonstrate the proposed method, an inservice pre-stressed concrete box bridge is examined. In particular, the seismic fragility curves of deteriorated bridges are compared with those of intact bridges. The numerical results show that the maximum failure probability of the deteriorated bridges is 3.6% higher than that of intact bridges. Therefore, the proposed method has the potential to updated the digital twin effectively using UAV inspection, allowing for seismic fragility analysis of deteriorated bridges to be conducted.

Keywords Seismic fragility analysis · Deteriorated bridge structure · Unmanned aerial vehicle (UAV) · Visual inspection · Bridge condition assessment · Digital twin

---

Responsible Editor: Zhen Hu

✉ Hyung-Jo Jung
hjung@kaist.ac.kr

1 Department of Artificial Intelligence, Hannam University, 70 Hannam-ro, Daedeok-gu, Daejeon 34430, Republic of Korea

2 Department of Urban and Environmental Engineering, Ulsan National Institute of Science and Technology, 50 UNIST-gil, Eonyang-eup, Ulju-gun, Ulsan 44919, Republic of Korea

3 Department of Civil and Environmental Engineering, Korea Advanced Institute of Science and Technology, 291 Daehak-ro, Yuseong-gu, Daejeon 34141, Republic of Korea

4 Department of Civil Engineering, Kunsan National University, 558 Daehak-ro, Kunsan 54150, Republic of Korea

5 Department of Civil and Environmental Engineering, University of Illinois at Urbana-Champaign, Urbana, IL 61801, USA

1 Introduction

A digital twin is an virtual model of the physical system reflecting the current status of the structure at any point in time (Hughes 2018). The three essential elements constituting the digital twin are: (1) the model of the target system, (2) measured data from the target system, and (3) the method of updating the target system with the measured data (Wright and Davidson 2020). Enabling the simulation of multi-physics, multi-scale, etc. through virtual physical models, the digital twin has received considerable attention from various academic fields. In addition, researchers have constructed a more powerful digital twin through acquisition of data using various sensors or images to update the physical model.

In the field of structural engineering, most of bridge structures have been in service for several decades; modeling without measured data from the as-built structure makes it difficult to predict the structural behavior. If serious damage

to bridges occurs, economic loss can result, leading to indirect damage of critical infrastructures (Yoon et al. 2018b, 2020). In particular, deteriorated bridges can result in a reduction of static and dynamic load capacities that differ from those considered in the as-built design, which can lead to unexpected structural responses under extreme loading conditions, such as earthquakes, floods, and wind (Fan et al. 2019, Camacho et al. 2020). For example, the I-35 W Mississippi River Bridge (built in the U. S. in 1961) and the Genoa Morandi Bridge (built in Italy in 1968), collapsed in 2007 and 2018, respectively, due to design flaw and structural deterioration. Therefore, maintenance or monitoring through acquisition of data from deteriorated bridges plays an important role in preventing serious accidents (Li and Zhang 2022; Wan et al. 2022).

For this reason, visual inspection of bridges using unmanned aerial vehicle (UAV) systems have recently attracted attention. For instance, Yoon et al. (2018a) evaluated the structural displacement using a UAV system, and Metni and Hamel (2007) proposed a visual surveying novel control law using UAV for monitoring and maintenance of bridges. In addition, Chen et al. (2019) adopted structure from motion (SfM) technology to reconstruct a 3-D bridge model and performed a visual inspection of the target bridge using images acquired from UAV. Their findings showed that using the proposed system, the cost and time required for visual inspection of bridges can be reduced compared to conventional methods, and the obtained data and point distribution results are more accurate. However, the proposed system showed low accuracy in the structural geometry and the detected damage due to the high noise level. To overcome this limitation, Jung et al. (2019b) developed a waypoint selection and path planning method through preflight, enabling the localization of acquired image data and mapping of the detected damage. Furthermore, Jung et al. (2019a) examined the major issues during bridge condition assessment using UAV and suggested solutions to overcome them.

However, previous studies have difficulties due to reliance on UAV pilot proficiency, external environmental factors such as weather and global positioning system (GPS) signals, and the use of commercial UAV systems. For this reason, researches have been conducted on developing enhanced UAV systems to acquire more accurate and consistent data in the face of these limitations. For example, Westoby et al. (2012) combined the pose of the camera and the image location, and also reconstructed a 3-D model of the target structure by introducing a novel feature detection methodology. Maria et al. (2005) evaluated the distance between the camera and the object using a laser meter to calculate the coordinates of the acquired images. In addition, Martínez et al. (2011) measured the facade dimensions of target structures by introducing close-range photogrammetry

(CRP) and a laser meter, and González-Aguilera and Gómez-Lahoz (2009) determined the shape of the target structure using a single image to obtain accurate and reliable data by employing perspective with three vanishings. Moreover, Yoon et al. (2021) calculated the center coordinates and region of interest (ROI) of local images acquired from various angles, taking into account the pose and position of the UAV and camera.

Recently, UAV images have been utilized to construct finite element (FE) model and conduct FE analysis through 3-D point cloud and photogrammetry reconstruction for structural monitoring and inspection. For instance, Morgenthal et al. (2019) proposed a comprehensive framework for automated UAV-based bridge condition assessment. In their research, a calibrated FE model was reconstructed through flight path and data acquired from UAV according to the structural shape, and the mechanical behavior of the modified FE model was investigated for bridge condition assessment. Bolourian and Hammad (2020) proposed an algorithm to minimize flight time by predicting potential damage locations using a LiDAR-equipped UAV system. To find the potential locations of the bridge damage, an FE analysis of the target bridge was performed, and the critical levels of the damages were classified based on the bridge response. In addition, Ozcan and Ozcan (2021) proposed an automated UAV system for evaluating multi-hazard analysis of bridges using the FE model from 3-D point cloud generation. Yoon et al. (2022) proposed a novel approach to assess the seismic response of bridges by employing UAV inspection-based damage detection. In their research, they evaluated the damage states of bridge components and updated the as-built design FE model.

However, data obtained from UAV in previous studies was utilized for FE model reconstruction, and how the detected damage affects structural behavior was not investigated. In particular, FE modeling was only performed by paying attention to the appearance change of the target structure through 3-D point cloud analysis, but the change in material properties of the structure according to the detected damage was not considered. In general, changes in the material properties of structural components shows unpredictable structural response against earthquake motion. Because various components (magnitude, duration, frequency contents, etc.) indicating the characteristics of an earthquake have many uncertainties, the response of the structure according to the specific hazard level cannot be calculated deterministically. Therefore, the seismic response of the structure should be estimated stochastically considering sufficient number of input earthquakes to include various seismic characteristics. Since changes in the material properties of structural components affect the seismic behavior, integrating UAV-based damage detection results with structural degradation of the FE model is critical to predicting the deteriorated structural

behavior. For this reason, the UAV-based seismic fragility analysis of deteriorated bridge was focused on in this study.

In view of the above, the results of bridge condition assessment based on UAV inspection were utilized to update the intact bridge FE model for seismic fragility curve analysis in this study. To this end, UAV inspection and condition assessment of a deteriorated bridge structure are first conducted, and then the seismic fragility analysis is performed based on the updated digital twin. For this purpose, deep learning-based damage detection analysis was performed using image data obtained through UAV inspection, and the detected damage was considered as a decrease in material properties for the bridge FE model. Based on the proposed approach, seismic fragility curves of intact and deteriorated bridges were compared. This methodology not only allows engineers to understand the seismic behavior of deteriorated bridges, but also predicts and minimizes damage in advance under unpredictable extreme loads such as earthquakes. In the remainder of this paper, a detailed explanation of the proposed methodology is introduced in Sect. 2, and an experimental demonstration was performed on an actual bridge structure in Sect. 3. In Sect. 4, the results and conclusion of this study is summarized.

2 Proposed methodology

This section describes the model construction of the proposed methodology for the UAV inspection-based bridge condition assessment for updated digital twin and seismic fragility analysis. Figure 1 shows the flow chart of the proposed methodology. Note that an intact bridge FE model represents an as-built design bridge model, and updated digital twin represents deteriorated bridge FE model.

For the UAV inspection for the updated digital twin, once the target bridge is determined, the flight path and visual inspection scenario are determined through preliminary information analysis. Based on acquired images from the UAV survey, it is determined whether any missing areas have occurred in the ROI. If the missing area is not detected, deep learning-based damage detection is performed with the acquired images and the damage grade and corresponding
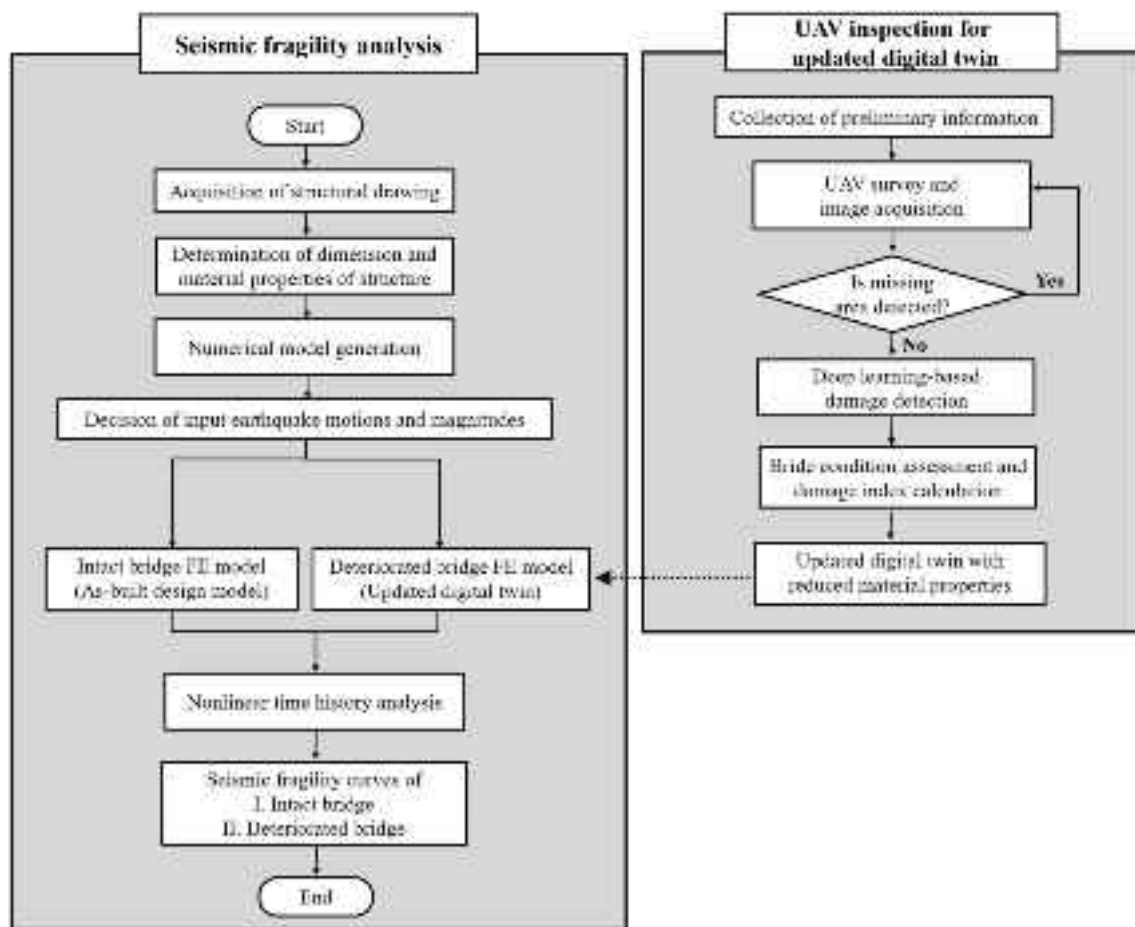

Fig. 1 Flow chart of proposed UAV inspection-based seismic fragility analysis model

damage index are calculated. Then, the damage index is reflected in the intact bridge FE model for the updated digital twin.

In the seismic fragility analysis, when the target bridge is determined, numerical modeling of the intact bridge is generated in consideration of the shape, dimensions, and material properties of the structure according to the structural drawing. Once the numerical model is generated, then the input earthquake motions and magnitudes are determined to consider the uncertainty of ground motion. Then, the input earthquakes are implemented in the intact bridge FE model and the deteriorated bridge FE model for nonlinear time-history analysis, respectively. Through seismic fragility analysis of each FE model, it is possible to evaluate the seismic fragility curve according to predefined damage states.

2.1 UAV inspection for updated digital twin

2.1.1 Image acquisition and damage detection

This section introduces the phase of updating the digital twin through UAV inspection-based bridge condition assessment. First, in order to perform a UAV inspection of the bridges, the target bridge should be determined for preliminary information analysis. The preliminary information analysis includes identification of material types (e.g., concrete, steel, etc.) or construction type (e.g., steel box, girder, etc.) and determination of inspection scenarios, flight paths, and camera setup including lenses according to local environmental conditions. After the collection of preliminary information, the next step is image acquisition through a UAV survey. In this step, acquiring images without missing areas in the entire ROI and obtaining high-quality images are important. To find missing area, first the coordinate transformations are conducted two times: (i) UAV-based coordinate system to camera-based coordinate system and (ii) camera-based coordinate system to world coordinate system, using GPS and inertial measurement unit (IMU) data of UAV and camera system to consider the location and posture of the UAV and camera. Then, the center coordinates of each field of view (FOV) can be calculated and the missing area can be detected by plotting each of the FOVs (in-plane). The details of image coordinates calculation using GPS and IMU data can be found in previously published paper (Yoon et al. 2020). If the missing area image has severe damages, it can influence the results of bridge condition assessment. Therefore, it is necessary to investigate the need for additional UAV surveys by identifying the missing region of a target structure.

For efficient damage detection, the mask region-based convolutional neural network (R-CNN) algorithm was introduced (He et al. 2017). Mask R-CNN algorithm, which is initially developed from CNN algorithm for image analysis, is combination of faster R-CNN model and fully convolutional network (FCN) to perform the object masking and localization simultaneously. First, the region proposal network (RPN) conduct object detection with image and then the Mask R-CNN extracts the object features map with ROI Align to perform the classification and mask representation. Because the mask branch is added for segmentation mask in Mask R-CNN algorithm, it gives accurate object detection results deriving from segmentation at the pixel level. For this reason, the Mask R-CNN algorithm is a very powerful deep learning algorithm that detects damage of civil infrastructure such as bridges because it finds the location of bridge damage based on the trained dataset (Kim and Cho 2019). With segmentation of damage by the mask R-CNN algorithm, accurate crack length and width, and damage area can be identified. In addition, the algorithm extracts not only the labeled damages, but also the various damage features for training. It efficiently constructs the training network even when training data are insufficient by adopting a back propagation method for updating the weight function. To train the R-CNN dataset in this study, damage detection of concrete structures was classified into 6 types of damage (i.e., crack, rebar exposure, water leak, breakage, material segregation, and efflorescence). For training the damage dataset, approximately 4,000 images were utilized, and the trained deep learning model was validated through 700 images (Kim et al. 2022).

2.1.2 Damage index calculation for updated digital twin

Once the damage is detected and quantified through deep learning, bridge condition assessment should be performed. For this purpose, the five damage grades of A to E in South Korea were adopted (Oh et al. 2001) and only the external damage of the target structure from UAV inspection was used to determine the bridge damage grade. In South Korea, the damage grade is classified according to crack damage and non-crack damages (MOLIT 2019, 2020). Note that damage grade D or E was not considered in this study because the vehicle or people's access is limited in those damage grade conditions.

In case of crack damage (Table 1), one-way crack and two-way crack (network crack) are distinguished to evaluate the damage as shown in Fig. 2. First, in case of one-way crack damage, for crack rate greater than 2% or less than 10% or for crack width between 0.3 and 0.5 mm, the bridge structure is classified as grade C. For crack width between 0.1 and 0.3 mm, the damage grade of the structure is grade B, and for crack width less than 0.1 mm, it is classified as grade A. On the other hand, in case of a two-way crack, if the crack width is greater than 0.3 mm, the damage grade is categorized as grade C. For crack width between 0.1 and

Table 1 Damage grade determination for crack damage

Grade	One-way crack	Two-way crack
A	Crack width < 0.1 mm	
B	0.1 mm ≤ Crack width < 0.3 mm	
C	2% ≤ Crack rate < 10%	Crack width ≥ 0.3 mm
	0.3 mm ≤ Crack width < 0.5 mm	

Table 2 Damage grade determination for non-crack damage

Grade	Surface damage	Rebar corrosion
A	No damage	No corrosion
B	Damage area < 2%	–
C	2% ≤ Damage area < 10%	Corrosion area > 2%

Table 3 Damage grade of bridges and corresponding damage index

Damage grade (For South Korea)	Damage state (Shinozuka et al. 2003)	Damage index (Shinozuka et al. 2003)
A	No	0
B	Minor	0.1
C	Moderate	0.3
D	Major	0.75
E	Collapse	1.0

0.3 mm, it is regarded as grade B, and finally, for crack width less than 0.1 mm, it is considered as grade A. The damage grade for the representative crack damage is assigned as the lower grade between the grades of the one-way crack and the two-way crack. In case of non-crack damage (Table 2), surface damage or rebar corrosion area is considered for the damage grade. The damage grade for surface damage area is classified as B if the area is less than 2% or C if the area is greater than 2% and less than 10% (grade A when no damage), and the area of rebar corrosion is assigned as grade C if the area is greater than 2% (grade A and B when no corrosion). Similar to crack damage, the representative grade of non-crack damage is determined as the lower grade among damage area of surface and rebar corrosion. The final damage grade is determined as the lower representative grade between crack damage grade and non-crack damage grade.

In this study, damage state and damage index are incorporated suggested by Shinozuka et al. (2003) to represent the updated structural response according to the damage grade. In their research, the damage state of the bridge was classified into five damage states, collapse damage, major damage, moderate damage, minor damage, and no damage based on the documentation of Hanshin Expressway Public Corporation (HEPC), which was reported using the empirical data on damage from the Kobe Earthquake. To incorporate the damage states and damage index, first, the damage grade is determined from UAV inspection, and then the corresponding damage state and following damage index are decided using Table 3. In Table 3, both definitions of damage grade and damage state are considered as the same description

as they are both classified into 5 levels from damage grade A ~ E and no damage to collapsed damage state, which represents that the quantitative damage is comparable. Therefore, in this study, the bridge damage index is incorporated with the bridge damage grade.

Previous researches have been conducted on the relationship between structural damage and elastic modulus to understand the structural behavior of deteriorated structures. For example, Pandey and Biswas (1994) adopted the changes in flexibility matrix (inverse of stiffness matrix) to detect and locate the structural damage, and Zimmerman and Kaouk (1994) employed the relationship between changes of stiffness and damage index to find the location and extent of structural damage and they demonstrated the developed algorithm by using actual experimental data and a finite element model. In addition, Barroso and Rodriguez (2004) conducted the structural identification of damaged four-story shear building structure (with stiffness and mass value), and damage index was utilized to evaluate the severity and

Fig. 2 Example of **a** one-way crack and **b** two-way crack

(a)   (b)

location of damage. Furthermore, other researchers have proposed and focused on the relationship between damage index reduction in the elastic modulus to understand the behavior of entire structure, and conducted experimental demonstration based on actual experimental data (Cha and Buyukozturk 2015; Duque 2017; Tan et al. 2017). In their study, they showed that the various structural damage have a complex relationship with reductions in stiffness to represent the damaged structural behavior. This study assumed that damage index was considered same as percent reduction in elastic modulus, because most of the bridges in service condition do not reach the severe damage condition and behave within the linear elastic range. For this reason, in this study, the damage index and damage states proposed by Shinozuka et al. (2003) were introduced to conduct a seismic fragility analysis of deteriorated bridges. In addition, the linear percent reduction of stiffness is considered the same as the damage index (Yoon et al. 2022), and the structural components of the intact bridge FE model are updated to reflect the deterioration of the current bridge structure.

2.2 Seismic fragility analysis

This study adopted a numerical model-based fragility analysis method to assess seismic fragility of a deteriorated bridge. In the method, a numerical model is constructed, and nonlinear time-history analysis is performed using the numerical model. Based on the results of nonlinear time-history analysis, failure probabilities are calculated comparing to given capacity limits. Iterative nonlinear time-history analysis is required to obtain failure probabilities at varying earthquake ground motion intensities (Yoon et al., 2019; Lee et al., 2016).

To perform seismic fragility analysis on deteriorated bridges, it is necessary to construct a numerical model of an as-built design bridge. For numerical modeling, obtaining the shape and dimensions of the structure, the state of the reinforcement, and the material properties based on the structural drawing is necessary. In addition, a simplified model and a full model can be considered according to the type or condition of the bridge, and depending on the structural behavior, a numerical model is constructed with a 2-D or 3-D model. For simplicity, the 3-D beam-stick model was constructed in consideration to the accuracy of the numerical results and the efficient numerical time for nonlinear time-history analysis. If the input earthquake motions are determined, the seismic fragility analysis can be conducted using the intact bridge FE model and the deteriorated bridge FE model. Subsequently, those seismic fragility curves can be derived based on each damage state as described in Fig. 1.

Seismic fragility curves are a probabilistic indicator of structural safety against earthquakes, which presents failure probabilities with varying intensities of earthquake ground motions. The failure probability (P_f) defines the conditional probability of the seismic demand (D) exceeding capacity (C) given an intensity measure (IM) as presented in Eq. 1 (Padgett and DesRoches 2008):

$$P_f = P[D \geq C | IM]$$ (1)

To calculate failure probabilities, nonlinear time-history analysis is performed using a FE model. The analysis is repeated to estimate structural responses in varying IM values. Based on the results, a probabilistic seismic demand model (PSDM) is derived by linear regression of the seismic responses and corresponding IM values such as Peak ground acceleration (PGA), Peak ground velocity (PGV), etc. (Mackie and Stojadinović 2005). Note that the PSDM is widely used to derive seismic fragility curves of bridge structures (Nielson and DesRoches 2007; Mangalathu et al. 2018). The seismic demand (D) is assumed to be the following approximation as presented in Eq. 2 (Cornell et al. 2002), where a and b are the parameters of the demand model.

$$D = a \cdot IM^b$$ (2)

The equation can be expressed as a linear equation in the natural logarithmic space as presented in Eq. 3. By a linear regression analysis, the unknown parameters of a and b are calculated.

$$\ln(D) = \ln(a) + b \cdot \ln(IM)$$ (3)

The logarithmic dispersion of the demand given IM, $\beta_{D|IM}$, can be obtained by Eq. 4 (Nielson and DesRoches 2007). In the equation, d_i is the peak value of the demand computed by nonlinear time-history analyses, and N is the total number of input ground motions.

$$\beta_{D|IM} \cong \sqrt{\frac{\sum_{i=1}^{N} \left(\ln(d_i) - \ln(D)\right)^2}{N - 2}}$$ (4)

Assuming both the demand and capacity to be lognormal distributions, the failure probability in Eq. 1 is expressed as the following equation. In the equation, S_D and S_C are the median values of the demand and capacity, respectively, β_C is the logarithmic dispersion of the capacity, and $\Phi(\cdot)$ is the standard normal cumulative distribution function.

$$P_f = P[D \geq C | IM] = \Phi\left(\frac{\ln(S_D) - \ln(S_C)}{\sqrt{\beta_{D|IM}^2 + \beta_C^2}}\right)$$ (5)

Fig. 3 Target region of bridge for UAV inspection

3 Experimental demonstration

3.1 Target bridge and UAV system

For experimental demonstration, the target bridge and the UAV system are explained in this section. The target bridge structure is the Deungsun bridge located in South Korea with a span length of 2,000 m and width of 11 m, and the total number of spans is 40 with 50 m maximum span length. The bridge was constructed around the 1980s, which is classified as a deteriorated bridge as it was built more than 40 years ago, and thus the earthquake-resistance design was not adopted. The superstructure of the bridge is composed of pre-stressed concrete (PSC) box type, and the target region of the bridge has two-segmented spans with three piers. Figure 3 shows the Deungsun bridge, and the black dashed rectangle shows the target region for UAV inspection.

To acquire the images of the target bridge, a newly developed UAV system was utilized. First, GPS and IMU sensors were attached to the UAV for UAV location and attitude estimation. To compensate for the vibration of the camera due to the movement of the UAV, a gimbal system was installed between the UAV and camera, and an IMU sensor for camera attitude was also attached. In addition, a full-frame camera sensor with 8 K resolution which is equipped with an 85 mm single lens was adopted to acquire high-resolution images. Moreover, the 1-D LiDAR sensor was installed to evaluate the distance between camera and object, and an LTE modem was attached to send signals to the UAV system. Figure 4 represents the UAV system for bridge inspection described above. Details of the developed UAV system can be found in the following documentation (Kim et al. 2022; Yoon et al. 2022).

3.2 Bridge condition assessment and damage index assignment

For image acquisition, the UAV inspection was conducted on the superstructure (bridge girder) and substructure (pier front surface and lateral surface) maintaining a distance of

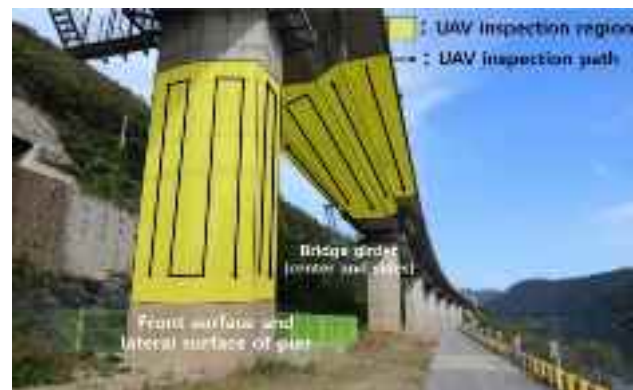**Fig. 4** Developed UAV system for bridge inspection

Fig. 5 UAV inspection region and flight path for updated digital twin

2.5 m between the UAV system and the target region. Figure 5 represents the UAV inspection region and flight path for an updated digital twin. To avoid the missing area in the inspection region, the acquired images are set to 70% overlapping area (rate) between each image. For flight path determination, the width and length of a bridge pier and a bridge girder were considered. In case of the front surface of the pier, the UAV system moves upward and downward two times to acquire the images of an entire region and one time for the lateral surface of the pier and bridge girder. Figure 6

shows the results of detection of missing area in bridge pier. Most of the regions were covered by each FOV, however, some parts of the edge were not detected. In this study, the missing area was minor and did not have significant effect on damage grade evaluation for damage detection purpose. These results showed that no additional UAV surveys are required to acquire the images of the missing area.

Figure 7 represents the results of UAV inspection on the front and lateral surface of the bridge pier and bridge girder. Although the mask R-CNN was trained and classified with 6 types of damage (crack, efflorescence, breakage, water leak, material segregation, and rebar exposure), the detected damage was only crack damage as seen in Fig. 7. The trained mask R-CNN model showed that the results of detection is 76.15% in recall with the standard intersection over union (IoU) of 50% and the precision was over than 95% for crack damage. For rebar exposure, the precision and recall was 100% and 71.4% respectively. In case of the breakage (including material segregation) the precision and recall was 100% and 88.8%, and the precision and recall was 100% and 100% for efflorescence damage. For accuracy of location, width, and length of the detected crack damages, the detected damage was compared with human visual inspection (Kim et al. 2022), and the comparison showed good agreement between both detection results. Using the detected crack damage, the bridge condition assessment was conducted according to the procedures described in Sect. 2.1.2 (MOLIT 2019, 2020). Table 4 shows the results of the bridge condition assessment, which is represented in terms of damage grade, damage index, and corresponding reduction in stiffness. The damage index was utilized to update the digital twin by reducing the stiffness of each component.
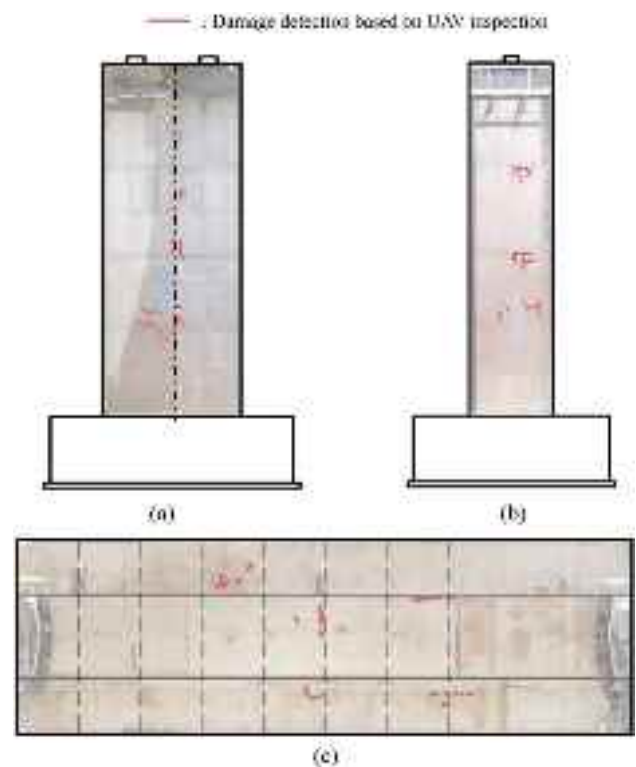

Fig. 7 Results of UAV inspection **a** front surface of bridge pier **b** lateral surface of bridge pier **c** bridge girder
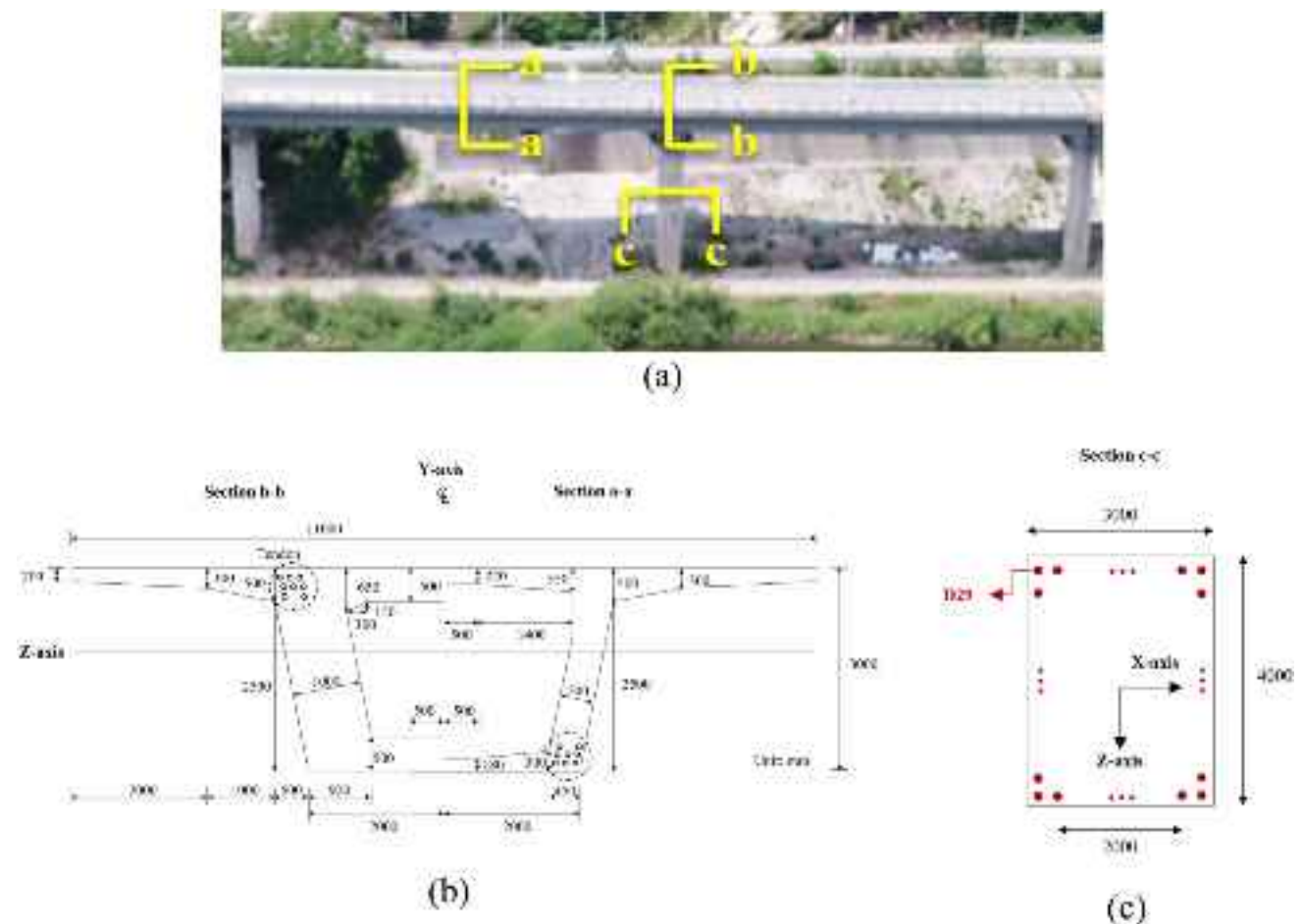
3.3 FE model generation

The objective of this study is to assess the seismic fragility of a deteriorated bridge, and for comparative purposes, the seismic fragility of an intact bridge is further investigated. The target structure is a PSC bridge, which is comprised of a single box girder and reinforced concrete (RC) piers. Details of cross-sections of the PSC box girder and the bridge pier are presented in Fig. 8.

Fig. 6 Missing area detection in ROI **a** front surface of pier **b** lateral surface of pier

Table 4 Bridge damage grade of target structure

Bridge region	Damage grade	Damage index	Reduction in stiffness (%)	Stiffness
30th pier	B	0.1	10	15.75GPa
31st pier	C	0.3	30	12.25GPa
32nd pier	C	0.3	30	12.25GPa
30th girder (sides)	C	0.3	30	12.25GPa
30th girder (center)	B	0.1	10	15.75GPa
31st girder (sides)	C	0.3	30	12.25GPa
31st girder (center)	B	0.1	10	15.75GPa

An FE model of the target bridge was constructed using Zeus-NL, which is an advanced FE analysis software package specializing in nonlinear dynamic analysis (Elnashai et al. 2010). The numerical modeling was performed based on a structural drawing of the target bridge. Figure 9 shows the simplified three-dimensional representation of the target bridge. In this study, an eccentric beam model was employed to conduct iterative nonlinear time-history analysis efficiently (Chan and Chan 1999). In the eccentric beam model, beam and truss elements are used to represent the structural behavior of slabs, girders, and PSC tendons by simplifying the complex behavior of full composite structures using rigid link elements. Previous studies validated the eccentric beam model by performing numerical modeling of slab on girder bridges (Chan and Chan 1999), composite steel girder bridges (Chung and Sotelino 2005), and PSC girder bridges (Chung et al. 2005), which was compared with experimental demonstration. The PSC box girder and RC pier are modeled by a three-dimensional cubic element with a concrete rectangular box section and an RC rectangular section, respectively, provided in Zeus-NL. PSC tendon was rigidly connected to the box girder, and pre-tension load to the tendon was applied to represent pre-stressing of the box girder. A joint element was employed to describe the relationship of the pier and girder, and an equivalent spring element was utilized to model the boundary conditions at each side

(a)

(b)

(c)

Fig. 8 **a** Location of each cross-section, and details of **b** PSC box girder (section a-a and section b-b) and **c** bridge pier (section c–c)
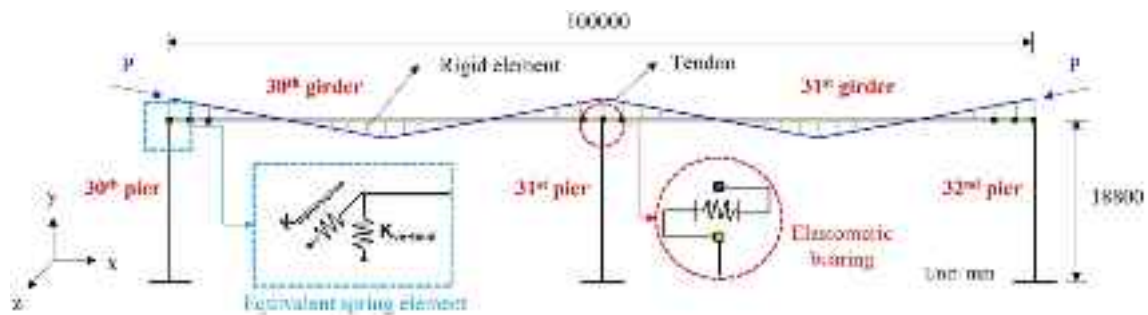
Fig. 9 Simplified three-dimensional model of the target bridge

(Wilson and Tan 1990). In piers, vertical reinforcing steel bars were modeled to be 29 mm in diameter with 150 mm intervals. The concrete and reinforcing steel were modeled by a uniaxial constant confinement concrete model and a bilinear elasto-plastic model with kinematic strain-hardening model, respectively (Elnashai et al. 2010). Figure 10 shows stress–strain curves of each material, and the strength of concrete is 35 MPa and the one of steel is 400 MPa. The application of such models to consider nonlinear behavior of concrete and steel can be found in previous studies (Moon et al. 2018 and Lee et al. 2021). For the numerical modeling of the deteriorated bridge, the damage index was used as a percent reduction in elastic modulus, which is experimentally demonstrated by previous research (Yoon et al. 2022). For the material property of each bridge region, the reduced elastic modulus was applied to take into account the results of the deteriorated bridge in Table 4.

Figure 11 shows the mode shapes and natural frequencies for the first eight modes of the deteriorated bridge. Note that the x-axis, y-axis, and z-axis represent longitudinal, vertical, and lateral direction, respectively. The first two modes of the deteriorated bridge model were found in lateral and vertical directions without longitudinal directions. As the order increases, the dynamic characteristic of the model tended to be in the lateral direction. The calculated natural frequency of the FE model developed in this study was in a reasonable range compared with similar bridge specifications of span length and girder width (Li et al. 2014; Vicente et al. 2015). Table 5 presents results of natural frequencies of the deteriorated bridge with those of the intact bridge. The deteriorated bridge model had lower frequencies than the intact bridge model because of the reduction in stiffness.

3.4 Nonlinear time-history analysis

Using the deteriorated bridge FE model developed in this study, nonlinear time-history analysis was performed in this section. In the analysis, twenty input ground motions were utilized to consider the uncertainty of earthquake ground motions, and both horizontal components of each input ground motion were applied simultaneously. The ground motion of vertical direction is much smaller than that of the longitudinal and later directions, and thus, vertical acceleration was not considered in seismic analysis. Table 6 represents the selected input ground motions, and Fig. 12 shows acceleration response spectra with 5% damping for the selected input ground motions in both longitudinal and later directions. PGA was selected as IM,

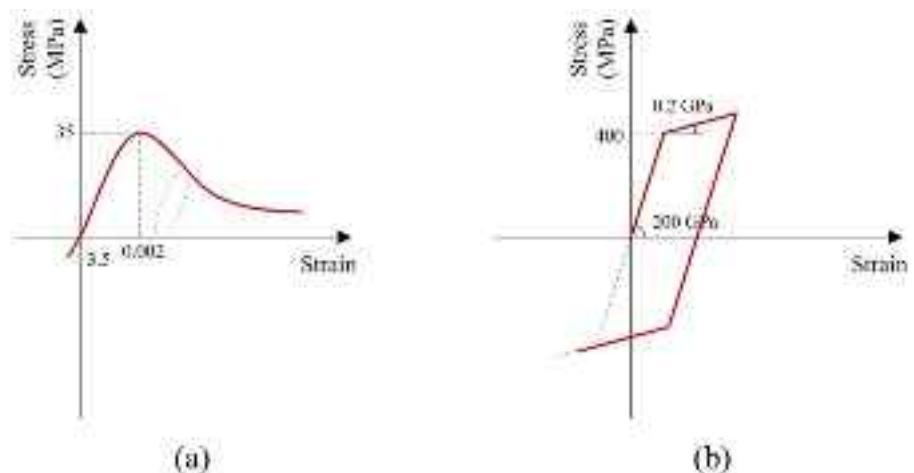**Fig. 10** Stress–strain curves of **a** concrete and **b** reinforcing steel
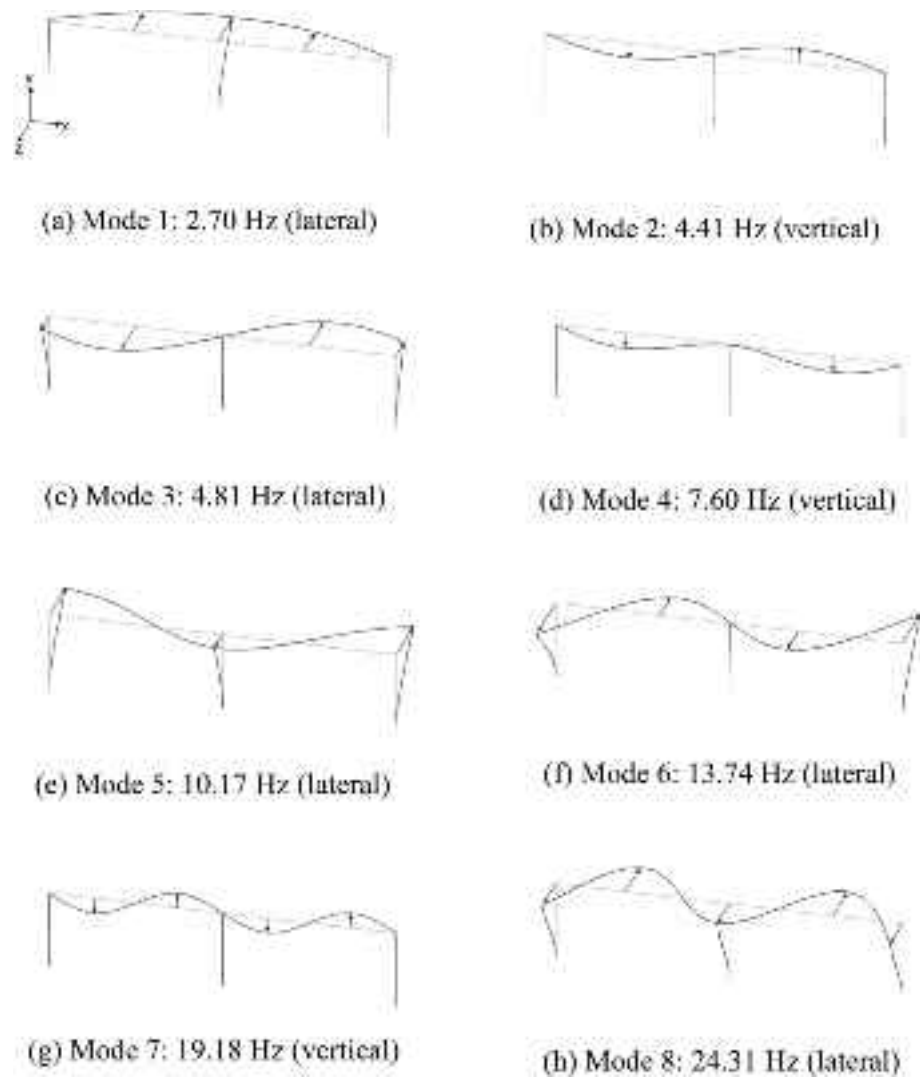
Fig. 11 Mode shape and natural frequencies of the deteriorated bridge

(a) Mode 1: 2.70 Hz (lateral)

(b) Mode 2: 4.41 Hz (vertical)

(c) Mode 3: 4.81 Hz (lateral)

(d) Mode 4: 7.60 Hz (vertical)

(e) Mode 5: 10.17 Hz (lateral)

(f) Mode 6: 13.74 Hz (lateral)

(g) Mode 7: 19.18 Hz (vertical)

(h) Mode 8: 24.31 Hz (lateral)

Table 5 Comparison of natural frequencies (HZ) of the deteriorated and intact bridges

Mode	Deteriorated bridge	Intact bridge
1	2.70	2.92
2	4.41	4.75
3	4.81	5.25
4	7.60	8.29
5	10.17	11.05
6	13.74	14.80
7	19.18	20.94
8	24.31	26.46

and the input ground motions were scaled from 0.1 g to 1.0 g PGA levels with 0.1 g intervals to obtain sufficient structural responses.
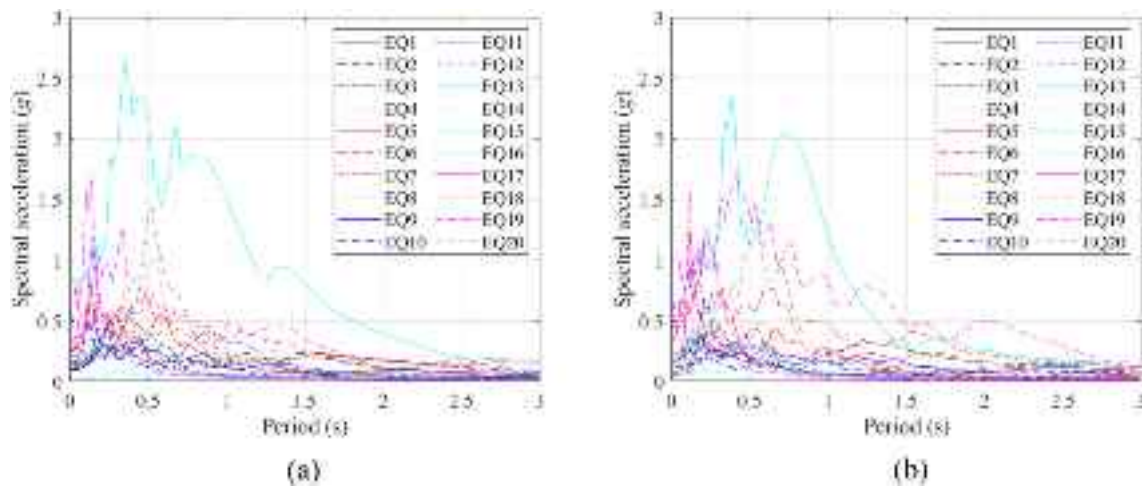
For the derivation of a seismic fragility curve, the drift ratio, which is defined as lateral displacement normalized by member height, was adopted to quantify the seismic demand based on the nonlinear time-history analysis. From the nonlinear time-history analysis, maximum drift ratios for each pier were evaluated at each PGA intensity. With pairs of the maximum drift ratios and corresponding PGA values, regression analysis was performed in the natural logarithmic space for each pier to derive PSDMs. Figure 13 shows PSDMs of the deteriorated bridge and the intact bridge, and Table 7 summarizes the parameters (*a* and *b*) determined from the regression analysis. The logarithmic dispersion of seismic demand, $\beta_{D|IM}$ was calculated for each pier using Eq. 4, and the results were presented in Table 8.

When comparing the seismic demand for the deteriorated and intact bridges, seismic demand for the deteriorated bridge was larger than that of the intact bridge. In Fig. 14, comparison results of PSDMs for the 31st pier are presented. As shown in the figure, it was identified that the deteriorated pier requires relatively large seismic demand than the intact pier at all PGA levels considered

Table 6 Selected twenty input ground motions for seismic fragility analysis

	Earthquake (Year)	Station	PGA (g)	Magnitude	Mechanism
EQ1	Gulf of Aqaba (1995)	Eliat	0.109	7.2	Strike slip
EQ2	Borrego (1968)	El Centro array #9	0.130	6.63	Strike slip
EQ3	Cape Mendocino (1992)	Eureka-Myrtle & West	0.178	7.01	Reverse
EQ4	Chi-Chi (1999)	CHY014	0.263	7.62	Reverse Oblique
EQ5	Chi-Chi (1999)	ILA067	0.198	7.62	Reverse Oblique
EQ6	Coalinga-01 (1983)	Park field Fault Zone 1	0.194	6.36	Reverse
EQ7	Imperial Valley (1979)	Delta	0.351	6.53	Strike slip
EQ8	Kocaeli (1999)	Fatih	0.187	7.51	Strike slip
EQ9	Landers (1992)	Indio-Coachella Canal	0.109	7.28	Strike slip
EQ10	Loma Prieta (1989)	Hayward-BART	0.159	6.93	Reverse Oblique
EQ11	San Fernando (1971)	Whittier Narrows Dam	0.107	6.61	Reverse
EQ12	Tabas (1978)	Ferdows	0.108	7.35	Reverse
EQ13	Kobe (1995)	KJM	0.821	6.9	Strike slip
EQ14	Duzce (1999)	Lamont 531	0.160	7.14	Strike slip
EQ15	Livermore (1980)	Antioch—510 G St	0.415	5.8	Strike slip
EQ16	Parkfield (2004)	CA—Gold Hill	0.171	6	Strike slip
EQ17	Iquique (2014)	Chusmiza, Chile	0.363	8.2	–
EQ18	Darfield (2010)	Canterbury Aero Club	0.198	7	Strike slip
EQ19	Gyeongju (2016)	USN2	0.433	(M_L) 5.8	–
EQ20	Pohang (2017)	PHA2	0.273	(M_L) 5.4	–

Fig. 12 Acceleration response spectra with 5% damping for the selected input ground motions in **a** longitudinal and **b** lateral directions

in this study. Therefore, the PSDMs derived using a large number of structural analysis results reflect the effect of deterioration, which contributes to realistically derive seismic fragility curves.

3.5 Seismic fragility curves

For seismic fragility curves, five damage states were considered; almost no, slight, moderate, extensive, and complete damage states. Drift limits for each damage state recommended by Dutta and Mander (1998) were used as presented in Table 9. The logarithmic dispersion of the capacity, β_C, was assumed to be 0.35 for all damage states, which was
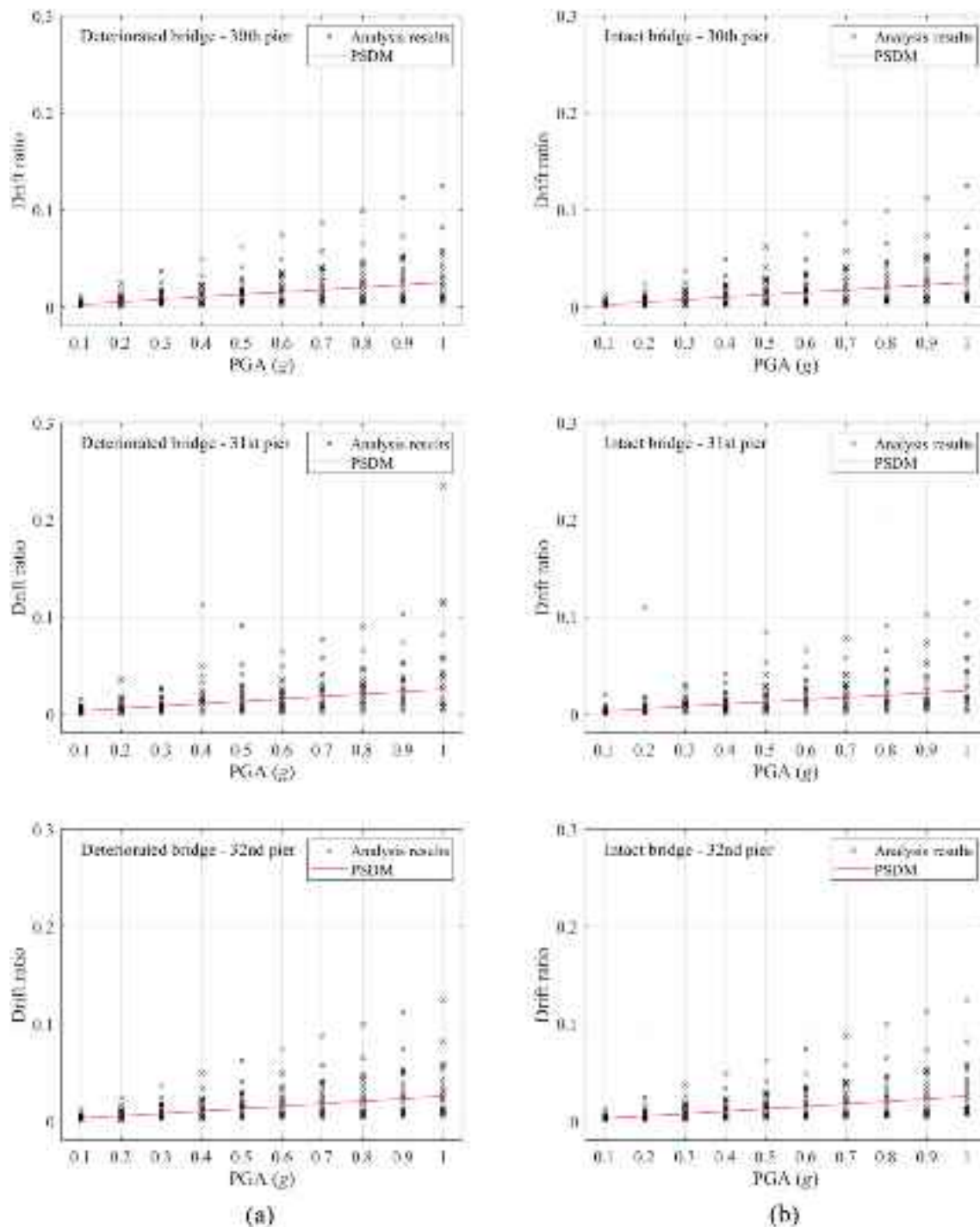
Fig. 13 PSDMs of **a** deteriorated and **b** intact bridges for each pier

a reasonable estimate for seismic fragility assessment of bridges (Ramanathan et al. 2015; Ghosh and Sood 2016).

From the calculated failure probabilities, seismic fragility curves were derived for each pier as presented in Fig. 15. In addition, the fragility curves of the deteriorated bridge were compared with those of the intact bridge. Overall failure
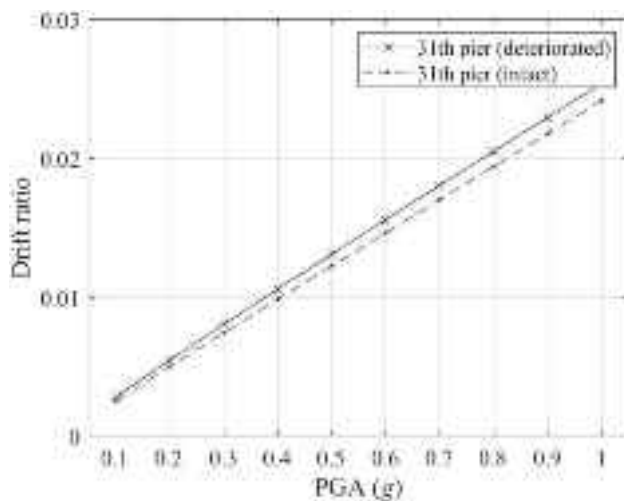
probabilities of the deteriorated bridge increased due to the detected crack damage which resulted in the reduction of elastic modulus. The damage grades of the 31st and 32nd piers were more severe than that of the 30th pier, but the structural response of the 30th and 32nd piers did not significantly influence the seismic fragility curve due to the

Table 7 Parameters of PSDMs

Bridge	Pier	Parameters	
		a	*b*
Deteriorated	30th	0.025305	0.996405
	31st	0.025355	0.954969
	32nd	0.025365	0.998111
Intact	30th	0.025272	1.024340
	31st	0.024110	0.979008
	32nd	0.025271	1.025463

Table 8 Logarithmic dispersion of seismic demand for each pier

Bridge	Pier	$\beta_{D|IM}$
Deteriorated	30th	0.859
	31st	0.944
	32nd	0.858
Intact	30th	0.871
	31st	0.935
	32nd	0.873

Fig. 14 Comparison results of the 31st pier PSDMs

Table 9 Drift limits for each damage state (Dutta and Mander 1998)

Damage state	Description	Drift limit (for non-seismically design)
Almost no damage	First yield	0.005
Slight damage	Cracking, spalling	0.007
Moderate damage	Loss of anchorage	0.015
Extensive damage	Incipient column collapse	0.025
Complete collapse	Column collapse	0.05

boundary condition of the PSC box girder (Note that both sides have equivalent spring element for connectivity). For this reason, a larger increase in failure probabilities was found at the 31st pier, and especially, the maximum difference of failure probability between the intact and deteriorated bridge was 3.6% at 0.1 g PGA, which was observed at almost no damage state. As the PGA increased, regardless of the damage state, the failure probability of deteriorated bridge was greater than that of an intact bridge. However, the effect of deterioration does not affect the failure probability of the intact and deteriorated bridges when the damage states are not severe after a certain PGA level (in case of almost no damage or slight damage).
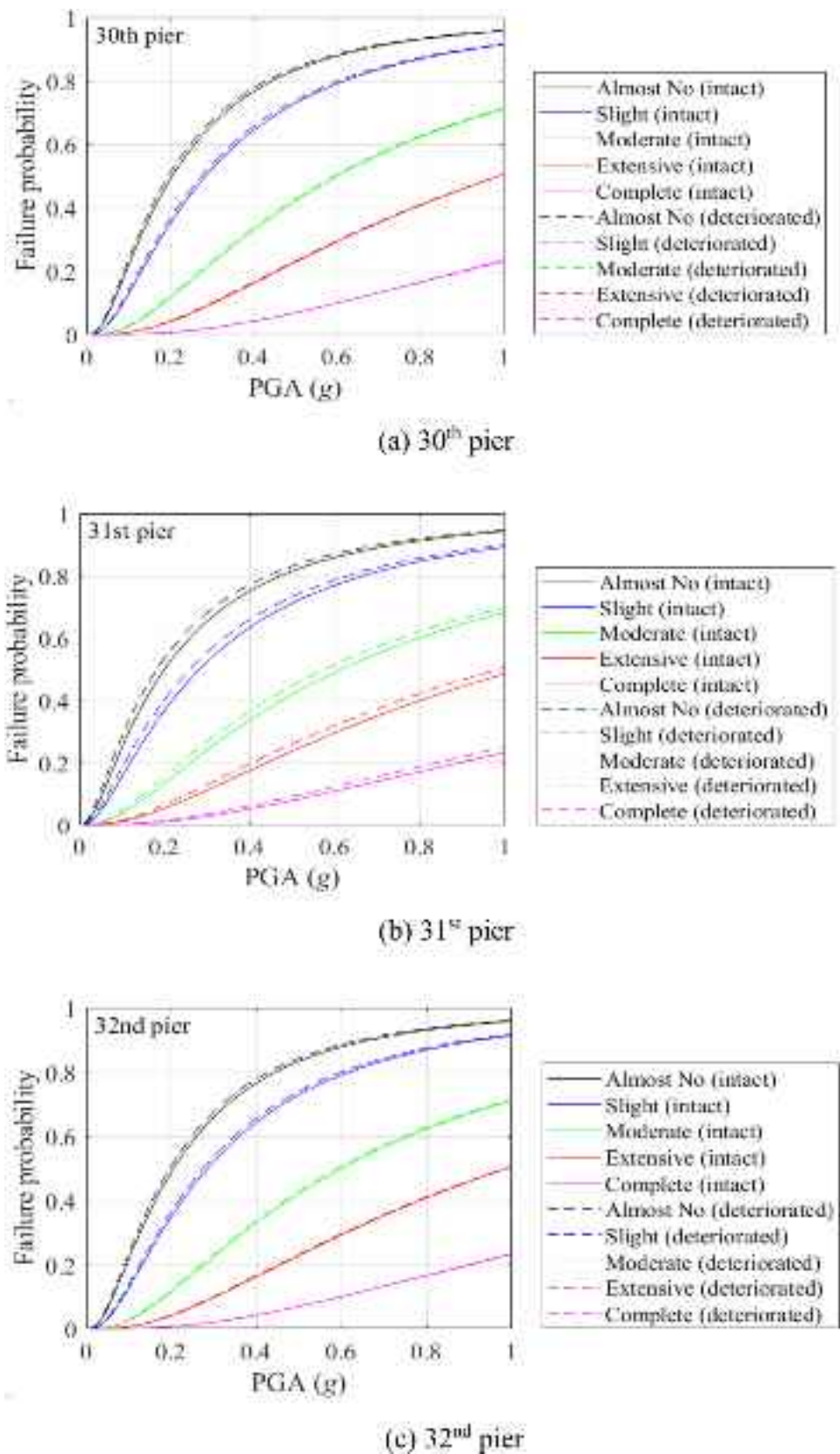
4 Discussion

The seismic fragility analysis methodology presented in this study has shown promising results and can be applied to various infrastructure systems in cooperation with more advanced UAV systems. However, further improvements will enable a more practical and accurate inspection of the structure. The further improvements include the UAV system, bridge damage grade and index, damage detection, and seismic fragility analysis. The main aspects of UAV inspection for updated digital twin and seismic fragility analysis in Fig. 1 have been highlighted and discussed in this section.

UAV system: Currently, a UAV-based inspection system only acquires images of the external surface of structures using a DSLR camera. However, if a UAV system is equipped with various sensors, for example, thermal imaging camera or non-destructive inspection equipment, it will be possible to inspect not only the exterior but also the interior of the structure. In addition, a UAV system with reliable access to target structures even in extreme conditions such as strong winds needs to be developed.

Bridge damage grade and index: To accurately evaluate the condition of deteriorated bridge structures, more detailed damage grades are needed from a practical point of view. In addition, the various damage types and damage sizes especially due to deterioration should be classified apart from other causes of damage to present detailed damage grades and corresponding damage index. In particular, a more accurate performance assessment of bridges will be possible by developing a continuous relationship (function) between the damage grade and the damage index for gradual damage index corresponding to damage grade.

Damage detection: By reducing the calculation time of damage detection, the system can perform bridge condition assessment with real-time identification of missing areas and damage grades. In addition, an advanced deep learning network should be developed to estimate the exact size and location of the damage on the structure and to quantify the

Fig. 15 Seismic fragility curves of the deteriorated and intact bridge

(a) 30th pier

(b) 31st pier

(c) 32nd pier

effect of the structural response of the detected damage on the structure. Finally, if low-quality images are enhanced to high-quality images with an image quality algorithm, an additional task such as re-flight can be reduced.

Seismic fragility analysis: Based on aspects mentioned above, the updated digital twin can be generated accurately and utilized for seismic fragility analysis. To consider the uncertainty of earthquake and structure, excessive nonlinear time-history analysis is necessary for seismic fragility curves. Therefore, the development of accelerated analysis techniques such as surrogate model is needed to derive the seismic fragility curve rapidly. In addition, for training the surrogate model, simplified numerical model enables reducing the nonlinear time-history analysis.

5 Conclusions

In this study, a methodology for seismic fragility analysis of deteriorated bridges employing a UAV inspection-based updated digital twin was proposed. The methodology consists of two phases: (1) UAV inspection for updated digital twin phase and (2) seismic fragility analysis phase. In the first phase, image acquisition and deep learning-based damage detection were performed based on UAV inspection, and damage index was assigned according to damage grade to update the digital twin. For model updating, the reduction in stiffness corresponding to the damage index of each structural component was applied to consider the damage grade in the FE model. In the second phase, numerical modeling of target structure was conducted using structural drawing, and the nonlinear time-history analysis of intact and deteriorated bridge FE model was performed to derive seismic fragility curves.

To demonstrate the proposed methodology, the Deungsun bridge (PSC box girder) located in South Korea was selected as the target structure. For image acquisition, a newly developed UAV system was utilized, and the crack damage was detected using the deep learning method. For seismic fragility analysis, a conventional method with a simple probability distribution function was utilized, and the failure probability was derived assuming lognormal distributions for both seismic demand and capacity. The seismic demand of the target bridge was analyzed through PSDMs, capacity limits for each damage state presented by a previous study were adopted. The results of the seismic fragility analysis showed that the failure probability of the deteriorated bridge was greater than those of the intact bridge because the elastic modulus of the deteriorated bridge was reduced due to detected damage. It was observed that a greater increase in failure probability was at the 31st pier and the maximum value was 3.6% at 0.1 g PGA at almost no damage state. So far, the proposed methodology was demonstrated on single

bridge structure for rapid seismic fragility analysis based on UAV inspection. Henceforward, the method can be used for efficient regular inspection of deteriorated bridges.

Declarations

Conflict of interest The authors declare that they have no conflict of interest.

Replication of results The results presented in this work can be replicated by implementing the UAV inspection-based damage detection and the finite element model. The data are available from the authors upon request.

References

Barroso LR, Rodriguez R (2004) Damage detection utilizing the damage index method to a benchmark structure. J Eng. Mech. 130(2):142–151

Bolourian N, Hammad A (2020) LiDAR-equipped UAV path planning considering potential locations of defects for bridge inspection. Autom Constr 117:103250

Cha YJ, Buyukozturk O (2015) Structural damage detection using modal strain energy and hybrid multiobjective optimization. Comput-Aided Civil Infrastruct Eng 30(5):347–358

Chan TH, Chan JH (1999) The use of eccentric beam elements in the analysis of slab-on-girder bridges. Struct Eng Mech 8(1):85–102

Chen S, Laefer DF, Mangina E, Zolanvari SI, Byrne J (2019) UAV bridge inspection through evaluated 3D reconstructions. J Bridg Eng 24(4):05019001

Chung W, Sotelino ED (2005) Nonlinear finite-element analysis of composite steel girder bridges. J Struct Eng 131(2):304–313

Chung W, Phuvoravan K, Liu J, Sotelino ED (2005) Applicabiliy of the simplified load distribution factor equation to PSC girder bridges. KSCE J Civ Eng 9(4):313–319

Cornell CA, Jalayer F, Hamburger RO, Foutch DA (2002) Probabilistic basis for 2000 SAC federal emergency management agency steel moment frame guidelines. J Struct Eng 128(4):526–533

Duque L (2017) UAV-based bridge inspection and computational simulations. South Dakota State University

Dutta A, Mander J (1998) Seismic fragility analysis of highway bridges. Proceedings of the INCEDE-MCEER center-to-center project workshop on earthquake engineering Frontiers in transportation systems.

Elnashai A, Papanikolaou V, Lee D (2010) Zeus-NL-A system for inelastic analysis of structures-user manual. Mid-America Earthquake (MAE) Center, Department of Civil and Environmental Engineering, University of Illinois at Urbana-Champaign, Urbana.

Ghosh J, Sood P (2016) Consideration of time-evolving capacity distributions and improved degradation models for seismic fragility assessment of aging highway bridges. Reliab Eng Syst Saf 154:197–218

González-Aguilera D, Gómez-Lahoz J (2009) Dimensional analysis of bridges from a single image. J Comput Civ Eng 23(6):319–329

He K, Gkioxari, G, Dollár P, Girshick R (2017) Mask r-cnn. Proceedings of the IEEE international conference on computer vision, p 2961–2969.

Hughes A (2018) Forging the digital twin in discrete manufacturing, a vision for unity in the virtual and real worlds. LNS Research e-book

Jung H-J, Lee J-H, Yoon S, Kim I-H (2019a) Bridge Inspection and condition assessment using unmanned aerial vehicles (UAVs): major challenges and solutions from a practical perspective. Smart Struct Syst Int J 24(5):669–681

Jung S, Song S, Kim S, Park J, Her J, Roh K, Myung H (2019b) Toward Autonomous Bridge Inspection: A framework and experimental results. 2019b 16th International Conference on Ubiquitous Robots (UR), IEEE, p 208–211.

Kim B, Cho S (2019) Image-based concrete crack assessment using mask and region-based convolutional neural network. Struct Control Health Monit 26(8):e2381

Kim I-H, Yoon S, Lee J-H, Jung S, Park JB, Jung H-J, Cho S (2022) A comparison study of human visual inspection method and UAS-based method on bridge inspection and condition assessment. Drones (Under review)

Lee DH, Kim BH, Jeong SH, Jeon JS, Lee TH (2016) Seismic fragility analysis of a buried gas pipeline based on nonlinear time-history analysis. Int J Steel Struct 16(1):231–242

Lee S, Moon D-S, Kim B, Kim J, Lee Y-J (2021) Hybrid fragility curve derivation of buildings based on post-earthquake reconnaissance data. Smart Struct Syst 28(4):553–566

Li X, Zhang N (2022) An efficient entropy-based global sensitivity analysis of bridge seismic demand based on a novel three-point-estimate method. Struct Multidiscip Optim 65(2):1–12

Li P-F, Wang Y-F, Liu B-D, Su L (2014) Damping properties of highway bridges in China. J Bridg Eng 19(5):04014005

Mackie K, Stojadinović B (2005) Comparison of incremental dynamic, cloud, and stripe methods for computing probabilistic seismic demand models. Structures Congress 2005: Metropolis and Beyond.

Mangalathu S, Choi E, Park HC, Jeon J-S (2018) Probabilistic seismic vulnerability assessment of tall horizontally curved concrete bridges in California. J Perform Constr Facil 32(6):04018080

Maria A, Tommaselli G, Luis M, Reiss L (2005) A photogrammetric method for single image orientation and measurement. Photogramm Eng Remote Sens 71(6):727–732

Martínez J, Ordóñez C, Arias P, Armesto J (2011) Non-contact 3D measurement of buildings through close range photogrammetry and a laser distance meter. Photogramm Eng Remote Sens 77(8):805–811

Metni N, Hamel T (2007) A UAV for bridge inspection: Visual servoing control law with orientation limits. Autom Constr 17(1):3–10

MOLIT (2019) Detail guidelines for safety inspections and full safety examinations. Ministry of Land Infrastructure and Transport, Korea Authority of Land and Infrastructure Safety

MOLIT (2020) Special act on the safety and maintenance of Facilities. Ministry of Land Infrastructure and Transport

Moon D-S, Lee Y-J, Lee S (2018) Fragility analysis of space reinforced concrete frame structures with structural irregularity in plan. J Struct Eng 144(8):04018096

Morgenthal G, Hallermann N, Kersten J, Taraben J, Debus P, Helmrich M, Rodehorst V (2019) Framework for automated UAS-based structural condition assessment of bridges. Autom Constr 97:77–95

Nielson BG, DesRoches R (2007) Analytical seismic fragility curves for typical bridges in the central and southeastern United States. Earthq Spectra 23(3):615–633

Oh B-H, Shin K-J, Kim K-S, Kim J-S, Lee S-C (2001) Improved criteria for condition assessment of bridges based on visual inspection. J Korea Inst Struct Maintenance Inspection 5(4):205–213

Ozcan O, Ozcan O (2021) Automated UAV based multi-hazard assessment system for bridges crossing seasonal rivers. Smart Struct Syst 27(1):35–52

Padgett JE, DesRoches R (2008) Methodology for the development of analytical fragility curves for retrofitted bridges. Earthquake Eng Struct Dynam 37(8):1157–1174

Pandey AK, Biswas M (1994) Damage detection in structures using changes in flexibility. J Sound Vib 169(1):3–17

Ramanathan K, Padgett JE, DesRoches R (2015) Temporal evolution of seismic fragility curves for concrete box-girder bridges in California. Eng Struct 97:29–46

Shinozuka M, Feng M, Kim H, Uzawa T, Ueda T (2003) Statistical analysis of fragility curves, Technical Report MCEER-03–002.

Tan ZX, Thambiratnam D, Chan T, Razak HA (2017) Detecting damage in steel beams using modal strain energy based damage index and artificial neural network. Eng Fail Anal 79:253–262

Vicente MA, González DC, Fu G (2015) Static and dynamic testing of high-speed rail bridges in Spain. J Bridg Eng 20(2):06014006

Wan L, Ouyang L, Zhou T, Chen Y (2022) An improved reliability-based robust design optimization method using Bayesian seemingly unrelated regression and multivariate loss function. Struct Multidisc Optim 65(2):1–16

Westoby MJ, Brasington J, Glasser NF, Hambrey MJ, Reynolds JM (2012) 'Structure-from-Motion' photogrammetry: a low-cost, effective tool for geoscience applications. Geomorphology 179:300–314

Wilson JC, Tan BS (1990) Bridge abutments: formulation of simple model for earthquake response analysis. J Eng Mech 116(8):1828–1837

Wright L, Davidson S (2020) How to tell the difference between a model and a digital twin. Adv Model Simulation Eng Sci 7(1):1–13

Yoon H, Shin J, Spencer BF Jr (2018a) Structural displacement measurement using an unmanned aerial system. Comput Aid Civil Infrastruct Eng 33(3):183–192

Yoon S, Lee Y-J, Jung H-J (2018b) A comprehensive framework for seismic risk assessment of urban water transmission networks. Int J Disaster Risk Reduct 31:983–994

Yoon S, Lee DH, Jung HJ (2019) Seismic fragility analysis of a buried pipeline structure considering uncertainty of soil parameters. Int J Press Vessels Pip 175:103932

Yoon S, Kim J, Kim M, Tak H-Y, Lee Y-J (2020) Accelerated system-level seismic risk assessment of bridge transportation networks through artificial neural network-based surrogate model. Appl Sci 10(18):6476

Yoon S, Gwon G-H, Lee J-H, Jung H-J (2021) Three-dimensional image coordinate-based missing region of interest area detection and damage localization for bridge visual inspection using unmanned aerial vehicles. Struct Health Monit 20(4):1462–1475

Yoon S, Spencer BF Jr, Lee S, Jung H-J, Kim I-H (2022) A novel approach to assess the seismic performance of deteriorated bridge structures by employing UAV-based damage detection. Struct Control Health Monit 29(7):e2964

Zimmerman DC, Kaouk M (1994) Structural damage detection using a minimum rank update theory. J Vibration Acoustic 116(2):222–231